Electronic Supplementary Material (ESI) for Nanoscale Advances.

Mechanical Anisotropy of Two-dimensional Metamaterials: A Computational Study

Ning Liu[1], Mathew Becton[1], Liuyang Zhang[2], Keke Tang[3] and Xianqiao Wang[1*]

[1]College of Engineering, University of Georgia, Athens, GA 30602 USA

[2] State Key Laboratory for Manufacturing Systems Engineering, Xi'an Jiaotong University, Xi'an, Shaanxi, 710049, China

[3] School of Aerospace Engineering and Applied Mechanics, Tongji University, Shanghai 200092, China

[*]Corresponding author: xqwang@uga.edu

Out-of-displacement Profiles at different strains

The out-of-plane displacement shown in Figure 2(b) is the maximum displacement of the whole structure. The out-of-plane displacement profiles at different strains for Figure 2(b) are shown in Figure S1. Consistent with Figure 2, when strain is below 0.2, the out-of-plane displacement over the whole structure is marginal. Beyond the critical strain 0.2, the out-of-plane displacement starts to increases rapidly. When strain is equal to 0.30, the maximum out-of-plane displacement is around 5 nm as seen in the black curve. Interestingly, the overall shape of the entire structure is in a sinusoidal shape from the loading direction.

Actually, the jump in strain-strain response in Figure 2(a) is caused by the out-of-plane buckling. Figure S2 shows the configurations of the 2D lattice structure at different strains. Consistent with Figure 2(b), the out-of-plane displacement for the entire structure is marginal when strain is below 0.2. During this stage, the axial group is stretched out under applied strain, leading to rotation of junctions and thus unbending the transverse group. The above deformation mechanism at the initial stage results in negative Poisson's ratio. However, around the critical strain, the bending energy stored in the transverse group is so large that the transverse group buckles in the z direction to release in-plane bending energy. As a result, the projection of transverse group in transverse direction starts to decrease, leading to positive Poisson's ratio. In fact, the out-of-plane buckling results from competition between out-of-plane bending and in-plane bending of transverse groups as shown in Figure 1(a). Near the critical point, the huge bending energy stored in the transverse group would induce out-of-plain buckling. As shown in Figure 4(b), 4(c) and 4(d), the bond and angle energy, an indicator of in-plane bending, experience a sharp drop while the dihedral energy, an indicator of out-of-plane buckling, experiences a sharp increase. Overall, the critical strain depends heavily on the ratio between out-of-plane bending stiffness and in-plane bending stiffness.

The effect of wavelength λ and bandwidth w

With respect to the effect of the overall MD model and each lattice ligament effect on the robustness of the results, additional simulations are performed and relevant results are shown here. Two geometrical parameters shown in Figure 1(a), namely wavelength λ and w, are studied here with respect to their corresponding effect on Poisson's ratio. The stiffness ratio between x and y direction is kept at 1 while the amplitude/wavelength ratio A is kept at 0.3. As seen in Figure S3 (a), strain-strain curves for structures with different wavelength λ share similar trend at the initial stage of the deformation, indicating that the corresponding Poisson's ratios are very close to each other. However, the critical strain where the Poisson's ratio starts to transition from negative to positive increases as the wavelength increases. Accompanying with the increase of wavelength λ, the in-plane bending stiffness grows closer to that of out-of-plane buckling, making the out-of-plane buckling difficult. Accordingly, the critical strain indicating the initialization of out-of-plane buckling also increases. Despite the significant influence on critical strain, wavelength λ plays a minor role in the Poisson's ratio of the 2D lattice structure as shown in Figure S3 (b), in which five independent runs with different initial velocity profiles are performed to get statistically meaningful data points. Similarly, width w also plays a very important role in determining the critical strain where Poisson's ratio starts to transition from negative to positive as shown in Figure S3 (c). When the width is 1.2 nm, no out-of-plane buckling happens, and Poisson's ratio is always below zero. As the width w increases, the in-plane bending stiffness increases proportionally to the third power of width w while the out-of-plane buckling increases linearly with the width w. Accordingly, the difference between in-plane bending stiffness and out-of-plane buckling stiffness increases, making the out-of-plane buckling easier and thus decreasing the critical strain where out-of-plane buckling happens. However, the width w has a marginal effect on the Poisson's ratio of 2D lattice structures as shown in Figure S3 (d) in which five independent runs are performed in a similar manner as that in Figure S3 (b). Those results are also in good agreement with the findings from a previous paper [1] that these two geometrical factors have limited influence on the magnitude of Poisson's ratio.

Model and simulation set-up for AA-MD simulations

The simulation box was fixed at 60 nm × 60 nm × 4nm, in which periodic boundary conditions were applied along x and y direction while a shrink-boundary condition was applied along z diretion. Amplitude A is equal to 0.3 while wavelength λ and band width w is 30 nm and 2.4nm, respectively. For both phosphorene and molybdenum disulfide, a modified Stillinger-Webber potential is used to describe interactions among atoms [2]. To perform a uniaxial tensile test, a strain-controlled loading method was adopted, in which a strain increment was added along the x direction every 10000 time steps via elongation of the box size while the lateral y direction was free to extend through a pressure control around 0 Pa. The resulting loading rate is around 1×10^{7} s^{-1}, falling into into the conventional strain rate regime (10^{7} to 10^{9} s^{-1}) as commonly used in molecular dynamics studies [3-5]. To eliminate the effect of thermal fluctuations, temperature was controlled around 1 K. Unless otherwise stated, time integration was performed on Nose-Hoover style non-Hamiltonian equations of motion from isothermal-isobaric (NPT) ensemble [6], in which time step was set to be 1 fs for stability and accuracy. All the simulations were performed by implementing a parallel solver for molecular dynamics LAMMPS [7] , and the results were visualized through the OVITO [8] package.

Figures

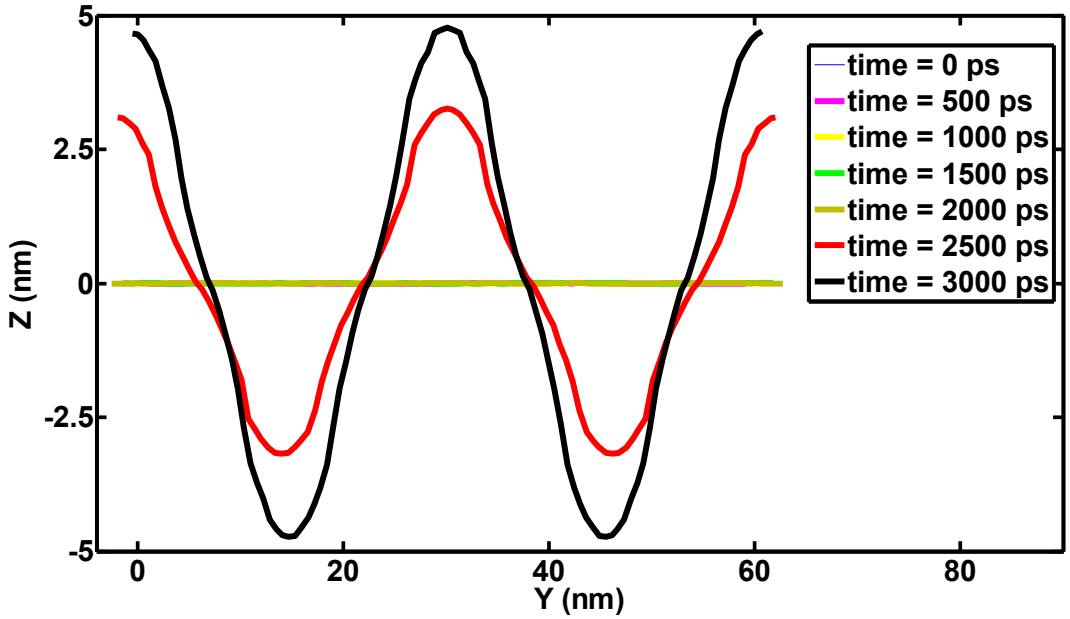

Figure S1 Corresponding out-of-plane displacement profiles at different strains extracted from the same set of simulation in Figure 2(b).

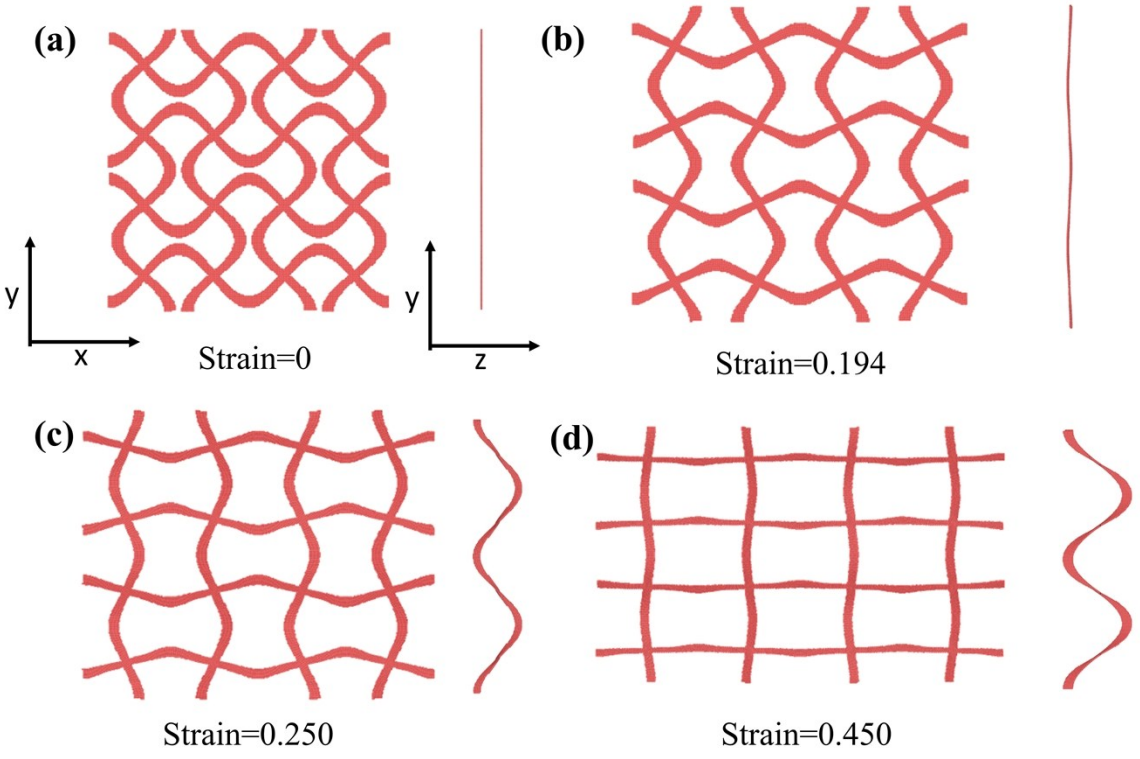

Figure S2 Geometrical configurations of the 2D lattice structure in Figure 2 at (a) strain = 0; (b) strain = 0.194; (c) strain = 0.250; (d) strain = 0.450.

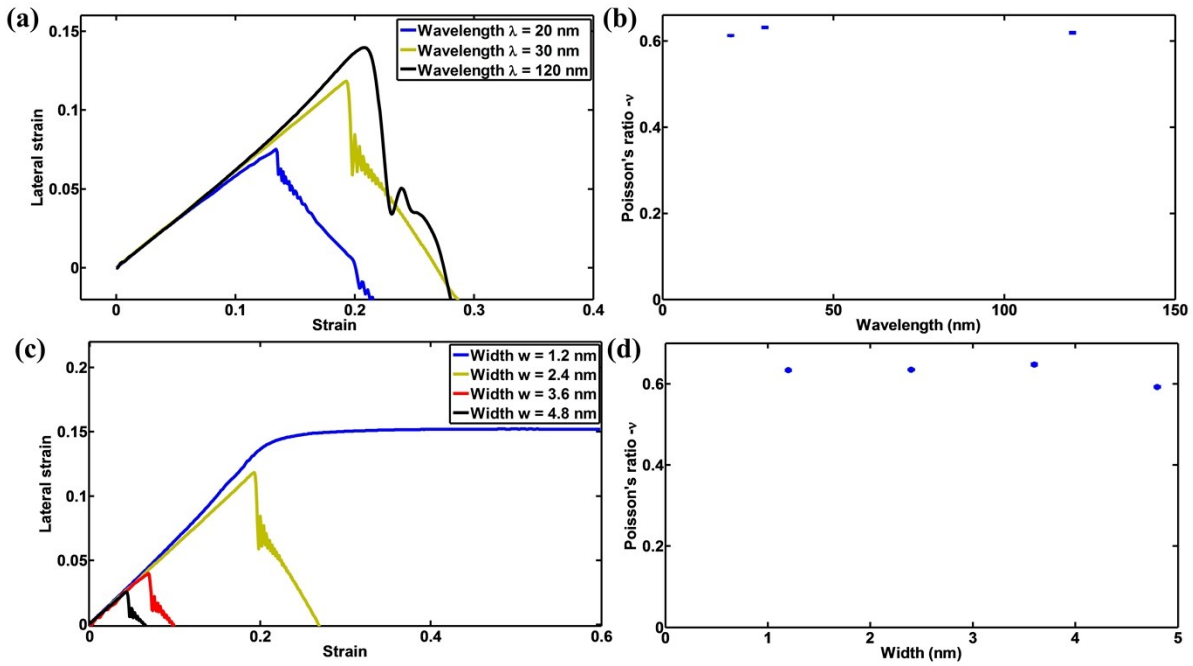

Figure S3 (a) Strain-strain relation for 2D lattice structures with different wavelength λ; (b) Poisson's ratio versus wavelength λ; (c) Strain-strain relation for 2D lattice structures with different width w; (d) Poisson's ratio versus width w.

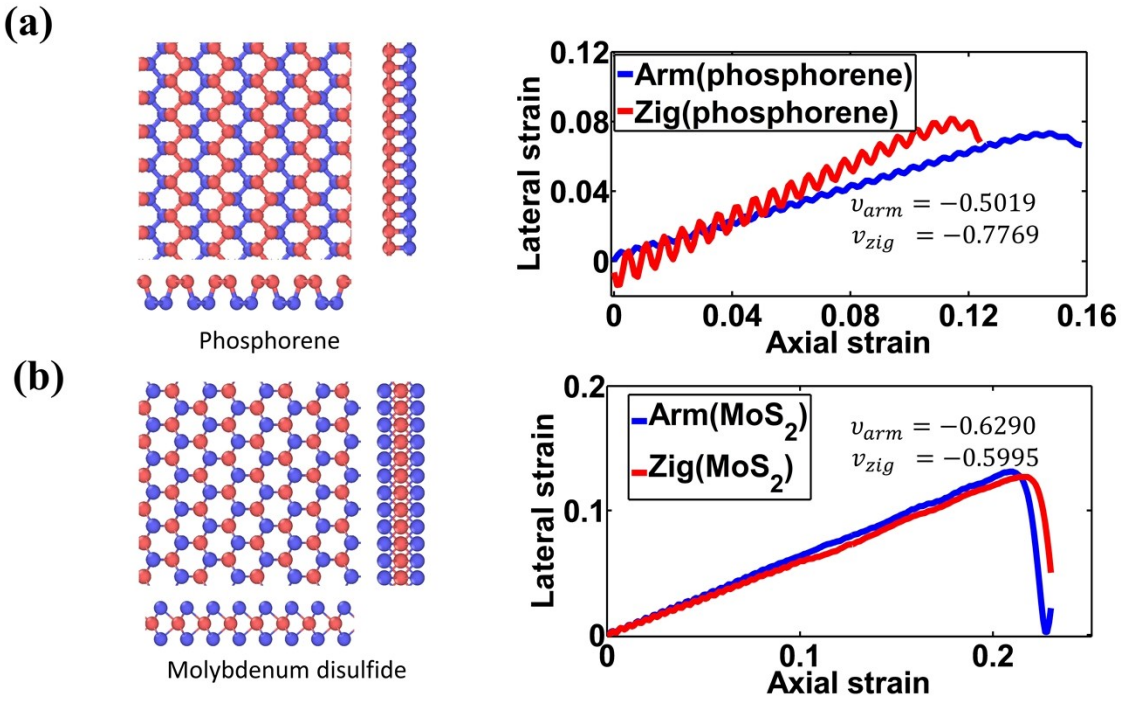

Figure S4. Strain-strain responses for (a) phosphorene; (b) molybdenum disulfide.

References

[1] Y. Chen, T. Li, F. Scarpa, L. Wang, Lattice Metamaterials with Mechanically Tunable Poisson's Ratio for Vibration Control, Physical Review Applied 7(2) (2017).
[2] J. Jin-Wu, Parametrization of Stillinger–Weber potential based on valence force field model: application to single-layer MoS 2 and black phosphorus, Nanotechnology 26(31) (2015) 315706.
[3] G. Jung, Z. Qin, M.J. Buehler, Molecular mechanics of polycrystalline graphene with enhanced fracture toughness, Extreme Mechanics Letters 2 (2015) 52-59.
[4] W.J. Xia, S. Keten, Size-dependent mechanical behavior of free-standing glassy polymer thin films, J. Mater. Res. 30(1) (2015) 36-45.
[5] T. Zhang, X. Li, S. Kadkhodaei, H. Gao, Flaw Insensitive Fracture in Nanocrystalline Graphene, Nano Letters 12(9) (2012) 4605-4610.
[6] E.T. Mark, A. José, L.-R. Roberto, L.J. Andrea, J.M. Glenn, A Liouville-operator derived measure-preserving integrator for molecular dynamics simulations in the isothermal–isobaric ensemble, Journal of Physics A: Mathematical and General 39(19) (2006) 5629.
[7] S. Plimpton, Fast Parallel Algorithms for Short-Range Molecular Dynamics, Journal of Computational Physics 117(1) (1995) 1-19.
[8] S. Alexander, Visualization and analysis of atomistic simulation data with OVITO–the Open Visualization Tool, Modelling and Simulation in Materials Science and Engineering 18(1) (2010) 015012.